technologies

MDPI

Article

Interfering Heralded Single Photons from Two Separate Silicon Nanowires Pumped at Different Wavelengths

Xiang Zhang [1,†], Runyu Jiang [1,†], Bryn A. Bell [1], Duk-Yong Choi [2], Change Joon Chae [3] and Chunle Xiong [1,*]

1 Centre for Ultrahigh bandwidth Devices for Optical Systems (CUDOS), Institute of Photonics and Optical Science (IPOS), School of Physics, University of Sydney, Sdyney 2006, NSW, Australia; b.zhang@physics.usyd.edu.au (X.Z.); runyu_jiang@hotmail.com (R.J.); bryn.bell@sydney.edu.au (B.A.B.)

2 CUDOS, Laser Physics Centre, Australian National University, Canberra 2601, ACT, Australia; duk.choi@anu.edu.au

3 Department of Electrical and Electronic Engineering, University of Melbourne, Melbourne 3010, VIC, Australia; cchae@unimelb.edu.au

* Correspondence: chunle@physics.usyd.edu.au; Tel.: +61-2-9351-5207

† These authors contributed equally to this work.

Academic Editor: Stephan Reitzenstein

Received: 13 July 2016; Accepted: 22 August 2016; Published: 24 August 2016

Abstract: Practical quantum photonic applications require on-demand single photon sources. As one possible solution, active temporal and wavelength multiplexing has been proposed to build an on-demand single photon source. In this scheme, heralded single photons are generated from different pump wavelengths in many temporal modes. However, the indistinguishability of these heralded single photons has not yet been experimentally confirmed. In this work, we achieve 88% ± 8% Hong–Ou–Mandel quantum interference visibility from heralded single photons generated from two separate silicon nanowires pumped at different wavelengths. This demonstrates that active temporal and wavelength multiplexing could generate indistinguishable heralded single photons.

Keywords: multiplexing; quantum optics; interference

1. Introduction

In the past two decades, quantum photonic technology has attracted significant attention due to its huge potential in applications such as secure communication [1], super-resolution metrology [2], and quantum computation [3]. However, the lack of efficient single photon sources is a major obstacle hindering the development of these applications. Several platforms [4–7] have been proposed to develop efficient single photon sources. One method is to use "single photon emitters" such as quantum dots [4] or nitrogen-vacancy (NV) centers in diamond [5]. Although these "single photon emitters" can generate single photons on-demand, photons generated from separate emitters are highly indistinguishable only after narrowband filtering [6]. Another method is to generate single photons in a nonlinear device via spontaneous nonlinear optical processes, such as spontaneous parametric down conversion (SPDC) [7,8] or spontaneous four-wave mixing (SFWM) [9,10]. In these nonlinear processes, two photons are generated simultaneously, and thus are correlated in time. The detection of one photon from a pair can herald the existence of its partner photon, forming a heralded single photon source. However, this method is intrinsically stochastic, and heralded photons generated in this way are not "on-demand": one cannot increase the probability of single-pair generation while simultaneously suppressing the probability of multi-pair generation.

Active multiplexing is an attractive way to overcome this intrinsic limitation of photon sources based on spontaneous nonlinear processes. One scheme is active spatial multiplexing, which collects single photons from many spatially-separated sources [11,12]. Similarly, active temporal multiplexing collects single photons generated in one nonlinear device but from many temporal modes [13–15]. Both schemes have been experimentally demonstrated [16–20] and have shown that the output probability of single photons can be enhanced [17–20]. Moreover, the indistinguishability of heralded single photons generated in these schemes has been verified [18,21]. Compared with spatial multiplexing, temporal multiplexing is a more promising solution, as there is a more favorable scaling of the physical resources with the number of modes. Figure 1a shows a schematic of active temporal multiplexing. The optical path of each heralded photon is controlled by a field programmable gate array (FPGA) according to the timing information of the heralding photon. In this scheme, if a large amount of temporal modes are multiplexed and an avalanche photon diode (APD) is used in the heralding channel, the APD can easily be saturated due to its long dead time, limiting the number of modes that can be multiplexed. One solution is to use superconducting single photon detectors (SSPD), which offers a much higher saturation margin, but the complex SSPD system which requires cryogenic temperatures to operate is not always available. Another feasible solution is to combine temporal and wavelength multiplexing, which can avoid detector saturation in the heralding channel [22], as the heralding photons are equally distributed into separate detector channels according to wavelength, as shown in Figure 1b. In our previous work [22], we have shown the advantage of this scheme using a silicon nanowire as the nonlinear device. However, as heralded photons are generated from different pump wavelengths, it is necessary to verify that these heralded photons are indistinguishable from one another. In this paper, we experimentally demonstrate Hong–Ou–Mandel (HOM) quantum interference [23] using heralded photons generated from two separate silicon nanowires pumped at different wavelengths. The interference exhibits 88% ± 8% visibility without subtracting any noise, indicating that these photons are highly indistinguishable. This demonstrates that the active temporal and wavelength multiplexing (ATWM) scheme is a possible solution to develop on-demand heralded single photon sources when only APDs are available.

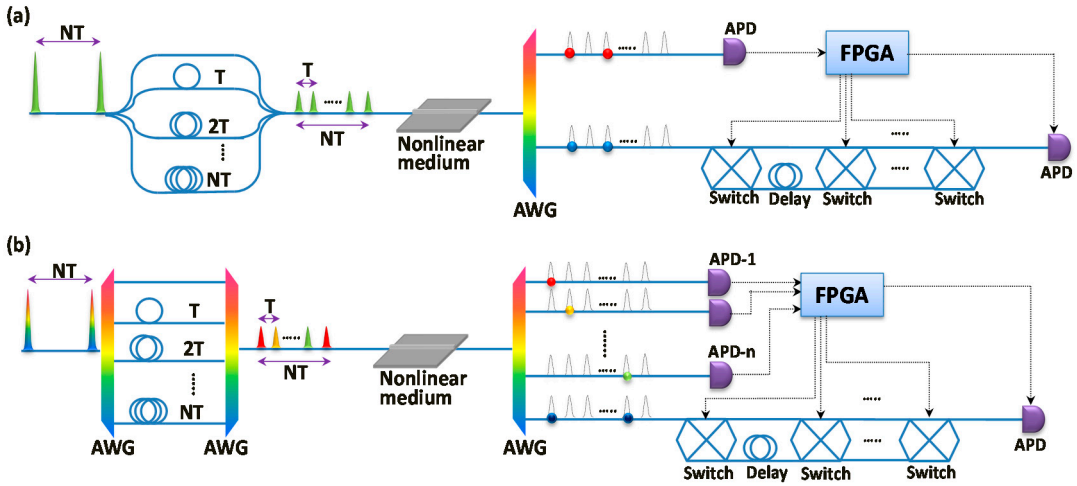

Figure 1. (**a**) Schematic of active temporal multiplexing. The light green pulses are pump pulses with narrow spectrum. The red ball represents a heralding photon, the dark blue one is the corresponding heralded photon. A field-programmable gate array (FPGA) controls delay routes of each heralded photon. APD: avalanche photon detector. (**b**) Schematic of active temporal and wavelength multiplexing. Colorful pump pulses indicate the wide spectrum. Red, yellow, and light green balls indicate heralding photons at different wavelengths. The dark blue ball represents a heralded photon. Blue lines represent optical fiber connections and black dashed lines denote electronic connection. The pulses after arrayed waveguide grating (AWG) indicate their timing information.

2. Experiment Methods

The enhancement of heralded single photon output rate [22] is not enough evidence to determine that ATWM is another possible multiplexing scheme, as the enhanced output rate does not necessarily indicate that these single photons are indistinguishable from one another. A rigorous verification, such as Hong–Ou–Mandel (HOM) quantum interference, is required to prove the indistinguishability of heralded photons generated from different pump wavelengths. To implement this verification, we use two nominally identical silicon nanowires pumped at different wavelengths and implement HOM interference between the heralded photons from each source. An alternative choice is pumping the same silicon nanowire with different pump wavelength and verifying the indistinguishability of heralded photons generated from different pump pulses and at different times. This would require splitting the heralded photon channel into two and relying on post-selection to overlap them in time for the HOM interference, so here we used two silicon nanowires.

The ATWM scheme requires the source have broadband SFWM so that the probability of creating heralded photons at a particular wavelength is similar for different pump wavelengths. Two silicon nanowires were used for our experiment; they were 3-mm-long, with a cross-section dimension of 220 $\times$ 460 nm, fabricated on silicon-on-insulator wafer with a 2 μm SiO_2 upper-cladding on top of the silicon nanowires. The transverse electric (TE) mode of silicon nanowires exhibits anomalous dispersion in the telecom band, and their SFWM bandwidth is more than 6 THz [22], potentially allowing for a large number of wavelength channels using standard telecom components.

The experimental setup is shown in Figure 2. The pump wavelengths of source A and source B were 1554.94 nm and 1555.74 nm, respectively. A standard telecommunication Gaussian-shaped arrayed waveguide grating (AWG) and tunable band pass filters (BPF) with a bandwidth of 0.4 nm and 0.8 nm, respectively, were used to separate two pump wavelengths from the same 50 MHz mode locked laser (MLL, original bandwidth 8 nm); then, the pump wavelengths were recombined and amplified in the same Erbium-doped fiber amplifier (EDFA). The pump wavelengths were separated again with an AWG and sent to the two silicon nanowire sources, with optical delay lines (ODL) to control the arrival times of the generated photons. Lensed fibers are used to couple to the silicon nanowires, which have inverse tapers on each end to further reduce the mode area mismatch between the fiber and nanowire. The average coupling loss of each facet was 2.5–3 dB. Polarization controllers (PC) before the nanowire were used to adjust the mode of pump wavelength. Correlated photon pairs from each nanowire were split into signal and idler channels by a Gaussian-shaped AWG and filtered by a tunable BPF with 3 dB and 2 dB insertion loss, respectively. The signal and idler wavelengths from source A were 1549.32 nm and 1560.60 nm, respectively. In source B, the wavelengths of signal and idler were 1550.92 nm and 1560.60 nm, respectively. The signal photons (1549.32 nm) generated in source A were detected by APD1, and the signal photons (1550.92 nm) generated in source B were detected by APD4. The idler photon (1560.60 nm) generated from sources A and B were detected by APD2 and APD3. The additional fibers before APD2 and APD3 behave as buffers, guaranteeing the heralded photons arrive at the detectors at the time when it is triggered by the heralding signals. The APDs were Id Quantique InGaAs ID210, with the detection efficiencies set to 25%, the dead time set to 10 μs, and the effective gate width equal to 1 ns. The total loss in each channel was around 15 dB, or 3.2% overall efficiency for each photon.

Before implementing HOM interference, we characterized both sources in terms of their coincidence to accidentals ratio (CAR) as the pump power is varied [24]. For the CAR measurement, idler photons from each source were sent directly to the APDs without the 50:50 coupler shown in Figure 2. Here, all four APDs were triggered by the electronic output of MLL, and a time interval analyzer (TIA) was used to record the coincidence rate and the accidental rate for each source.

After characterizing these two sources, we implemented both two-fold and four-fold HOM quantum interference, as discussed below. In the HOM dip measurements, idler photons were transmitted into a single 50:50 coupler via PCs, which were used to match their polarizations. In the two-fold HOM dip measurement, only two detectors (APD2 and APD3) were used, and were triggered

by the MLL clock. In the four-fold HOM dip measurement, all four detectors were used, with APD2 and APD3 triggered by heralding photon detections from APD1 and APD4.

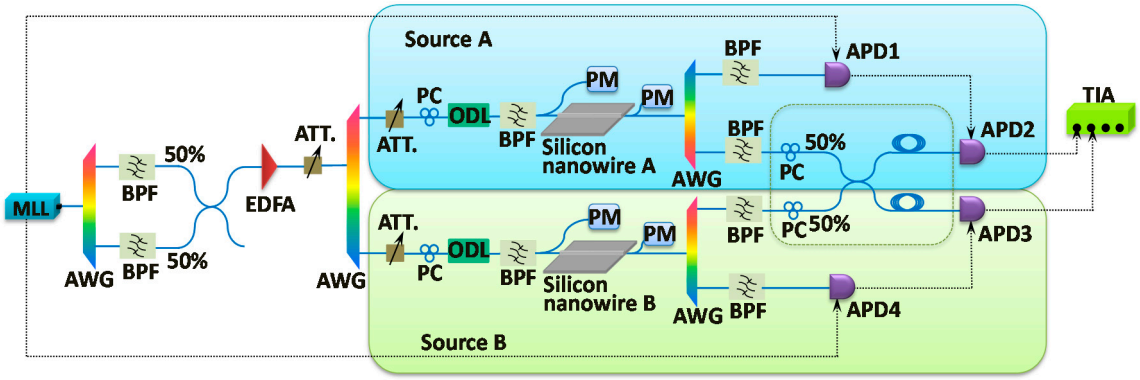

Figure 2. Experimental setup. The polarization controller (PC), 50:50 coupler, and additional fiber before avalanche photon diode APD2 and APD3 are only for the Hong–Ou–Mandel (HOM) quantum interference, and are removed for initial characterization of the sources. ATT is a tunable attenuator; BPF: band pass filter; EDFA: Erbium-doped fiber amplifier; MLL: mode locked laser; ODL: optical delay line; PM: power meter; TIA: time interval analyzer.

3. Results

The CAR measurement results are plotted in Figure 3a. The data points of source A and source B are very close to each other, which indicates the two sources are well balanced in brightness and CAR. They are both in good agreement with analytical results using the equation in Ref. [17], shown by the green dashed line. The analytical curve is higher than the experimental results when the coincidence rate is more than 600 Hz, which is caused by the 10 μs dead time of the APDs at high count rates. As the detected photon rate increases, there is more chance that a photon will arrive during the dead time created by a previous detection. This effectively leads to a drop in detector efficiency.

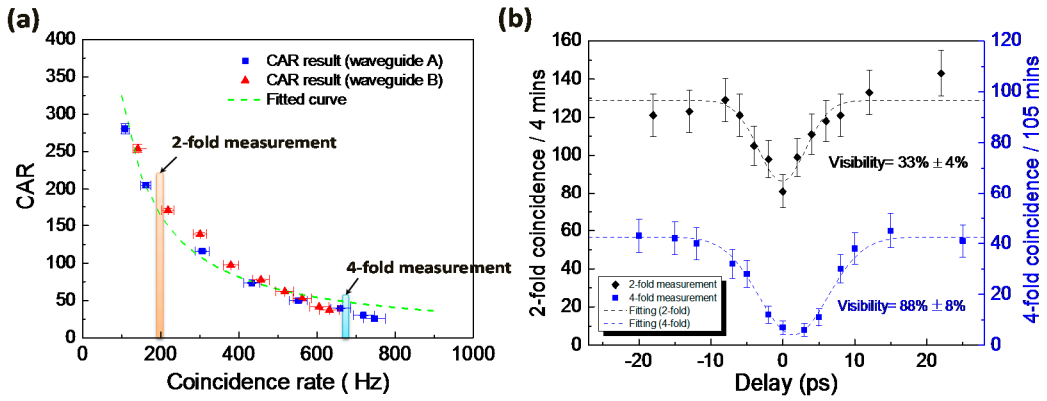

Figure 3. (**a**) coincidence to accidentals ratio (CAR) vs. coincidence rate. Blue rectangles: CAR measurement results in waveguide A; red triangles: CAR measurement results in waveguide B; green dashed line: analytical plot. Light red bar shows the experimental condition of two-fold HOM dip measurement, and light blue bar points the experimental condition of the four-fold HOM dip measurement; (**b**) two-fold and four-fold HOM dip experimental results. Black diamonds: two-fold experimental result; black dashed line: fitted curve using a Gaussian function. Blue rectangles: four-fold experimental results; blue dashed line: fitted curve using a Gaussian function.

After characterizing the two sources, we carry out two-fold and four-fold HOM quantum interference measurements, and the results are depicted in Figure 3b. In the two-fold HOM dip

measurement, the average power is set at 100 μW so that the coincidence rate is 156 Hz and CAR is 205, as indicated by the red bar in Figure 3a. Coincidences are accumulated for 4 min per data point, and the relative delay is varied using the ODL connected in source A. Based on a Gaussian function, the two-fold fitted curve in Figure 3b shows 33% ± 4% visibility, close to the theoretical limit of one third. In the four-fold experiment, the count rate is much lower than in the two-fold case, because of the loss and detector efficiency. Hence, we doubled the pump power of each source in order to increase the counts rate to around 600 Hz heralded single photons in APDs 2 and 3, as indicated by the blue bar in Figure 3a. The measurement time per data point is also increased to 105 min. The experimental result for the four-fold HOM dip is shown in Figure 3b with a fitted curve of 88% ± 8% visibility, without subtracting any noise. Here, the ideal maximum visibility should be 100% if there is no noise.

4. Discussion

The two-fold HOM dip is a coincidence measurement between the interfering modes, but without heralding information. In this case, coincidence events arise from three cases: a single photon from each of source A and B; two photons generated in source A; and two photons generated in source B. When the two sources are well balanced in their average number of photon pairs per pulse μ, the probabilities of the three cases all scale with μ^2, making the total coincidence events scale with $3\mu^2$. Only the case with one photon coming from each source can show HOM interference. Hence, the theoretical predication of the two-fold HOM visibility is one third, $(C_{Max} - C_{Min})/C_{Max} = (3\mu^2 - 2\mu^2)/3\mu^2$, where C_{Max} is the maximum coincidence rate which is seen away from the dip, and C_{Min} is the minimum coincidence rate, seen at the center of the dip. The two-fold HOM dip is a convenient method to find the exact delay at which the dip is positioned, because it can be carried out faster than the four-fold measurement. Here, the visibility is so close to the theoretical maximum that it gives us a good indication that the photons generated by different pump wavelengths are highly indistinguishable. However, four-fold HOM quantum interference requires that the heralding detectors be used, so that we know a single photon was generated in each channel for every coincidence. Hence, the four-fold experiment is a more rigorous demonstration of the quality of the sources.

For the four-fold measurement, only the cases with at least one photon from each channel remain, because of the heralding information. This includes the case with a single photon from each source, scaling with μ^2, which interfere perfectly. The multi-photon contributions—which scale with μ^n ($n \geq 3$)—will degrade the visibility of the HOM dip. Including only the terms of order μ^3, the theoretical visibility is expressed as [21]:

$$V = \frac{1 + 8\mu}{1 + 12\mu}$$

This gives a theoretical value of HOM dip visibility V = 94% for the inferred μ = 0.02 in our four-fold measurement. The $n > 3$ contributions are expected to be negligible. Another potential error source comes from residual spectral correlations between the signal and idler of a pair (which can reduce the visibility), but these should be avoided by the use of narrow spectral filtering on all of channels in the experiment. The experimental visibility of 88% ± 8% is within the error of this theoretical value (the error is based on the Poissonian statics of the count rates). This result demonstrates that non-classical single photon interference indeed takes place between two heralded single photons generated from different pump wavelengths, as the HOM dip visibility far exceeds the classical limit of 50%. Based on this work, we confirm that the ATWM scheme is a possible solution to building on-demand heralded single photon sources.

5. Conclusions

In this work, we demonstrate that heralded photons generated from two separate silicon nanowires pumped at different wavelengths are indistinguishable through 88% ± 8% visibility of HOM quantum interference. The residual distinguishability is likely due to the multi-pair noise

generated at high pump power. This shows that the ATWM scheme is able to enhance the single photon output probability of sources based on SFWM while maintaining the indistinguishability of the photons, which is essential to many applications in quantum communication and quantum computing. This takes us another step towards a practical, room temperature source of single photons.

Acknowledgments: We would like to thank Professor Benjamin Eggleton for his support to this project. The work is supported by the Centre of Excellence (CUDOS, CE110001018), Future Fellowship (FT110100853), Discovery Project (DP130100086) and Discovery Early Career Researcher Award (DE120100226) programs of the Australian Research Council (ARC). The project is partly supported by Huawei Technology Ltd.

Author Contributions: C.X. proposed and designed the experiment. X.Z. and R.J. setup the experiment, took the data and analyzed the data under C.X. and B.A.B's supervision. D.-Y.C and C.J.C provided the silicon nanowire. C.X. supervised the research throughout.

Conflicts of Interest: The authors declare no conflict of interest. The founding sponsors had no role in the design of the study; in the collection, analyses, or interpretation of data; in the writing of the manuscript, and in the decision to publish the results.

References

1. Marcikic, I.; Riedmatten, H.D.; Tittel, W.; Zbinden, H.; Gisin, N. Long-distance teleportation of qubits at telecommunication wavelengths. *Nature* **2003**, *421*, 509–513. [CrossRef] [PubMed]
2. Afek, I.; Ambar, O.; Silberberg, Y. High-NOON states by mixing quantum and classical light. *Science* **2010**, *328*, 879–881. [CrossRef] [PubMed]
3. Gottesman, D.; Chuang, I.L. Demonstration the viability of universal quantum computation using teleportation and single-qubit operations. *Nature* **1999**, *402*, 390–339.
4. Claudon, J.; Bleus, J.; Malik, N.S.; Bazin, M.; Jaffrennou, P.; Gregersen, N.; Sauvan, C.; Lalanne, P.; Gérard, J.-M. A highly efficient single-photon source based on a quantum dot in a photonic nanowire. *Nat. Photonics* **2010**, *4*, 174–177. [CrossRef]
5. Huck, A.; Kumar, S.; Shakoor, A.; Andersen, U.L. Controlled coupling of a single nitrogen-vacancy center to a silver nanowire. *Phys. Rev. Lett.* **2011**, *106*, 096801. [CrossRef] [PubMed]
6. Delteil, A.; Sun, Z.; Gao, W.B.; Togan, E.; Faelt, S.; Imamoglu, A. Generation of heralded entanglement between distant hole spins. *Nature Phys.* **2016**, *12*, 218–223. [CrossRef]
7. Ramelow, S.; Mech, A.; Giustina, M.; Gröblacher, S.; Wieczorek, W.; Beyer, J.; Lita, A.; Calkins, B.; Gerrits, T.; Nam, S.W.; et al. Highly efficient heralding of entangled single photons. *Opt. Express.* **2013**, *21*, 6707–6717. [CrossRef] [PubMed]
8. Jin, H.; Liu, F.M.; Xu, P.; Xia, J.L.; Zhong, M.L.; Yuan, Y.; Zhou, J.W.; Gong, Y.X.; Wang, W.; Zhu, S.N. On-chip generation and manipulation of entangled photons based on reconfigurable lithium-niobate waveguide circuits. *Phys. Rev. Lett.* **2014**, *113*, 103601. [CrossRef] [PubMed]
9. Xiong, C.; Collins, M.J.; Steel, M.J.; Krauss, T.F.; Eggleton, B.J.; Clark, A.S. Photonic crystal waveguides sources of photons for quantum communication applications. *IEEE J. Sel. Top. Quantum Eletron.* **2015**, *21*, 205–214. [CrossRef]
10. He, J.; Bell, B.A.; Casas-Bedoya, A.; Zhang, Y.; Clark, A.S.; Xiong, C.; Eggleton, B.J. Ultracompact quantum splitter of degenerate photon pairs. *Optica* **2015**, *2*, 779–782. [CrossRef]
11. Migdall, A.L.; Branning, D.; Castelletto, S. Tailoring single-photon and multiphoton probabilities of a single-photon on-demand source. *Phys. Rev. A* **2002**, *66*, 053805. [CrossRef]
12. Pittman, T.B.; Jacobs, B.C.; Franson, J.D. Single photons on pseudodemand from stored parametric down conversion. *Phys. Rev. A* **2002**, *66*, 042303. [CrossRef]
13. Jeffrey, E.; Peters, N.A.; Kwiat, P.G. Towards a periodic deterministic source of arbitrary single-photons. *New J. Phys.* **2004**, *6*, 100. [CrossRef]
14. Mower, J.; Englund, D. Efficient generation of single and entangled photons on a silicon photonic integrated chip. *Phys. Rev. A* **2011**, *84*, 052326. [CrossRef]
15. Shapiro, J.H.; Wong, F.N. On-demand single-photon generation using a modular array of parametric downconverters with electro-optic polarization controls. *Opt. Lett.* **2007**, *32*, 2698–2700. [CrossRef] [PubMed]
16. Ma, X.S.; Zotter, S.; Kofler, J.; Jennewein, T.; Zeilinger, A. Experimental generation of single photons via active multiplexing. *Phys. Rev. A* **2011**, *83*, 043814. [CrossRef]

17. Collins, M.J.; Xiong, C.; Rey, I.H.; Vo, T.D.; He, J.; Shahnia, S.; Reardon, C.; Krauss, T.F.; Steel, M.J.; Clark, A.S.; et al. Integrated spatial multiplexing of heralded single-photon sources. *Nat. Commun.* **2013**, *4*, 2582. [CrossRef] [PubMed]
18. Xiong, C.; Zhang, X.; Liu, Z.; Collins, M.J.; Mahendra, A.; Helt, L.G.; Steel, M.J.; Choi, D.-Y.; Chae, C.J.; Leong, P.H.W.; et al. Active temporal multiplexing of indistinguishable heralded single photons. *Nat. Commun.* **2016**, *7*, 10853. [CrossRef] [PubMed]
19. Kaneda, F.; Christensen, B.G.; Wong, J.J.; Park, H.S.; McCusker, K.T.; Kwiat, P.G. Time-multiplexed heralded single-photon source. *Optica* **2015**, *2*, 1010–1013. [CrossRef]
20. Mendoza, G.J.; Santagati, R.; Munns, J.; Hemsley, E.; Piekarek, M.; Martín-López, E.; Marshall, G.D.; Bonneau, D.; Thompson, M.G.; O'Brien, J.L. Active temporal and spatial multiplexing of photons. *Optica* **2015**, *2*, 127–132. [CrossRef]
21. Harada, K.; Takesue, H.; Fukuda, H.; Tsuchizawa, T.; Watanabe, T.; Yamada, K.; Tokura, Y.; Itabashi, S. Indistinguishable photon pair generation using two independent silicon wire waveguides. *New J. Phys.* **2011**, *13*, 065005. [CrossRef]
22. Zhang, X.; Jizan, I.; He, J.; Clark, A.S.; Choi, D.-Y.; Chae, C.J.; Eggleton, B.J.; Xiong, C. Enhancing the heralded single-photon rate from a silicon nanowire by time and wavelength division multiplexing pump pulses. *Opt. Lett.* **2015**, *40*, 2489–2492. [CrossRef] [PubMed]
23. Hong, C.K.; Ou, Z.Y.; Mandel, L. Measurement of subpicosecond time intervals between two photons by interference. *Phys. Rev. Lett.* **1987**, *59*, 2044. [CrossRef] [PubMed]
24. He, J. Degenerate photon-pair generation in an ultracompact silicon photonic crystal waveguide. *Opt. Lett.* **2014**, *39*, 3575–3578. [CrossRef] [PubMed]